INTEGRA

RICERCA & SVILUPPO

"A FIBRE ELEMENT FOR CYCLIC BENDING AND SHEAR. II: VERIFICATION"

Petrangeli, M. (1999)

FIBER ELEMENT FOR CYCLIC BENDING AND SHEAR OF RC STRUCTURES. II: VERIFICATION

By Marco Petrangeli[1]

ABSTRACT: The fiber beam element with shear modeling developed in the companion paper is calibrated and verified by comparison with test data. The verification is carried out for the material constitutive behavior and for single beam and column elements using available test results from literature. A structural analysis of a shear sensitive viaduct pier subjected to ground input motion is presented. Details of the algebraic expressions used for the concrete and steel constitutive behaviors are provided.

INTRODUCTION

Following the general theoretical formulation discussed in the companion paper (Petrangeli et al. 1999), calibration and verification of the new fiber beam model with shear modeling using test data available from literature is performed. A qualitative description of the section behavior is also presented to clarify the beam element mechanics with respect to the shear modeling and its interaction with axial and bending forces.

CONCRETE

The stress-strain law used for the microplane normal ''weak'' component is based on the work of Mander et al. (1988), which, in turn, used an equation suggested by Popovics (1973): The same law has been used by the writer (Petrangeli 1996) in the traditional fiber beam element for the uniaxial behavior of concrete. The skeleton curve in compression has the following expression:

$$s_k^w = \frac{f_{cc} x r}{r - 1.0 + x^r} \tag{1}$$

$$x = \frac{e_k^w}{\epsilon_{cc}}; \quad r = \frac{E_c}{(E_c - E_{\text{sec}})}; \quad E_{\text{sec}} = \frac{f_{cc}}{\epsilon_{cc}}$$

where f_{cc} = peak strength; ϵ_{cc} = corresponding strain; and E_c = initial elastic modulus.

The unloading branch is defined by the secant modulus E_{sec} that decreases as a function of the material damage. In the Mander model, damage is measured by the maximum compressive strain reached during the analysis. Calling with (ϵ_{un}, σ_{un}) the coordinates of the reversal point, the unloading branch is given by the following expression:

$$s_k^w = \sigma_{un} - \frac{\sigma_{un} x r}{r - 1.0 + x^r} \tag{2}$$

$$x = \frac{e_k^N - \epsilon_{un}}{\epsilon_{pl} - \epsilon_{un}}; \quad r = \frac{E_u}{(E_u - E_{\text{sec}})}; \quad E_{\text{sec}} = \frac{\sigma_{un}}{\epsilon_{pl} - \epsilon_{un}}$$

where E_u = unloading tangent modulus at reversal, decreasing as a function of the maximum compressive strain reached during the analysis; and ϵ_{pl} = inelastic strain (i.e., the residual strain at zero stress), which is given, according to Mander et al. (1988) by

$$\epsilon_{pl} = \epsilon_{un} - \frac{(\epsilon_{un} + \epsilon_a)\sigma_{un}}{(\sigma_{un} + E_c \epsilon_a)} \tag{3}$$

where the strain ϵ_a is, in turn, a function of the maximum strain reached during the analysis.

The reloading branch is linear elastic with a polynomial transition curve joining it to the skeleton curve. All of the unloading and reloading branches that do not exceed the maximum strain have the same secant modulus E_{sec} (i.e., there is no degradation in cycles of the same amplitude). A detailed description of the cyclic rules used in the model can be found in Mander et al. (1988), although some improvements and suggestions have been introduced according to the work of Martinez-Rueda and Elnashai (1997).

An example of the accuracy of the model under uniaxial cyclic stress history can be seen in comparison with the test results of Sinha et al. (1964) in Fig. 1.

The tensile branch of concrete is not a material property, but it depends on the reinforcement configuration and the corresponding stiffening energy dissipated by the concrete fiber. The following simple exponential expression has therefore been used:

$$s_k^w = E_c e_k^w \left(1 - e^{[-(e_k^w/e_1)^{p_1}]}\right) \tag{4}$$

where e_1 and p_1 = two parameters to be fixed according to the strength and fracture energy required. The tensile strength is a material parameter and is calibrated to match the material behavior in tension. The energy under the stress-strain diagram depends, as mentioned earlier, on the cross-sectional geometry and reinforcement configuration, and therefore, a different value may be specified for each concrete fiber.

Lateral expansion of the concrete section that takes place over the compression-shear range activates the stirrup confinement. This expansion, which increases with the material damage, can be caused by the material dilatancy due to large

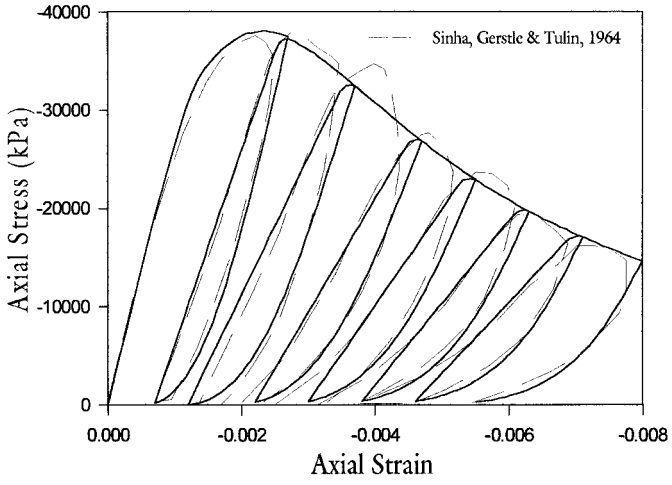

FIG. 1. Uniaxial Compression—Cyclic Behavior

[1]Asst. Prof., Facu. of Arch., Univ. ''G. D'Annunzio,'' 65127 Pescara, Italy.

Note. Associate Editor: Sunil Saigal. Discussion open until February 1, 2000. Separate discussions should be submitted for the individual papers in this symposium. To extend the closing date one month, a written request must be filed with the ASCE Manager of Journals. The manuscript for this paper was submitted for review and possible publication on January 7, 1998. This paper is part of the ***Journal of Engineering Mechanics***, Vol. 125, No. 9, September, 1999. ©ASCE, ISSN 0733-9399/99/0009-1002–1009/$8.00 + $.50 per page. Paper No. 17321.

longitudinal compressive strains as well as by the relative displacement across diagonal shear cracks. A mixture of the two is most likely to occur in a beam-column element as the result of bending, shear, and axial force coupling. The following tests demonstrate the model capability to correctly predict the response of a concrete specimen over the compressive-shear range.

The model dilatancy is strongly influenced by the ''strong-weak'' strain partitioning governed by the exponential expression proposed in the companion paper (Petrangeli et al. 1999)

$$\phi(\epsilon^{dam}) = e^{(\epsilon^{dam}/e_2)^p}; \quad \epsilon^{dam} = \epsilon^D \epsilon_2^{\max} \tag{5}$$

where ϵ^D = deviatoric invariant; and $\epsilon_2^{\max}$ = maximum compressive strain. For the e_2 constant, the $1.5\epsilon_{cc}^2 \leq e_2 \leq 1.0\ \epsilon_{cc}^2$ range, with ϵ_{cc} being the compression strain at peak load, seems to bracket the most common situations for concrete materials. For the p exponent instead (the larger its value the more brittle is the material response), a value equal to one has been assumed in all of the following tests. More refined expressions for the $\phi(\epsilon^{dam})$ function could be investigated, still retaining the main advantage of this function, which does not need to have cyclic capabilities because a loss of internal cohesion in the material is typically an irreversible process.

The first proposed simulation refers to the uniaxial compression test by van Mier (1986), shown in Fig. 2. The prediction of the model's lateral response is fairly good, taking into account that in the postpeak regime these types of test results are influenced by the structural response of the test specimen and cannot be taken as representative of the materials' behavior, even on a macroscale. Still, it is an undeniable concrete feature, which must be incorporated into the model, to have a Poisson's ratio almost constant up to peak load followed by a large dilatancy in the postpeak response.

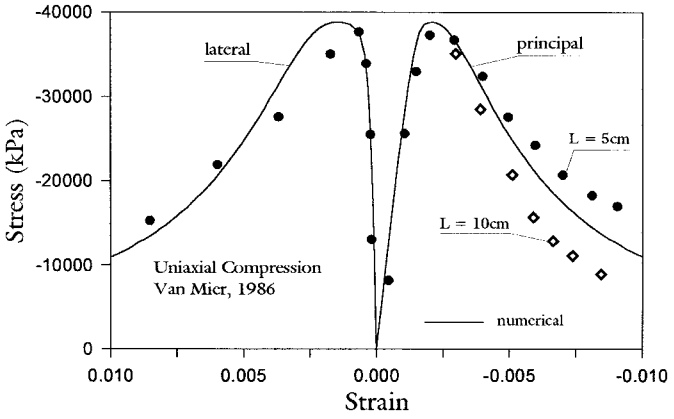

FIG. 2. Uniaxial Compression

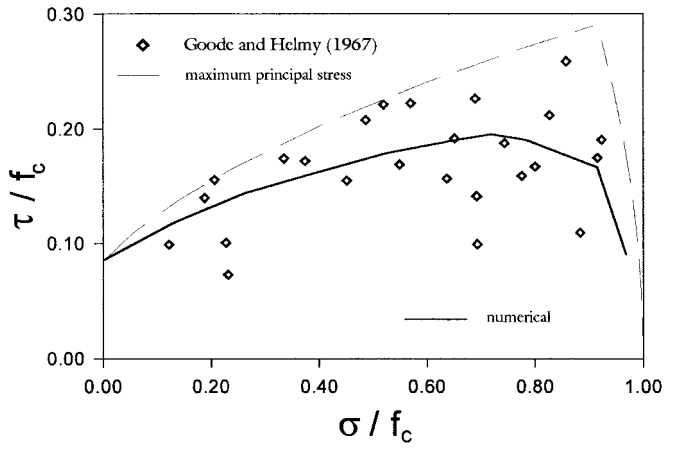

FIG. 3. Compression-Shear: Failure Envelope

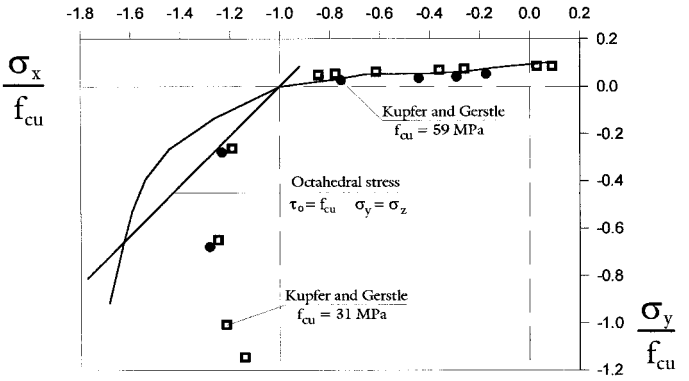

FIG. 4. Biaxial Compression Failure Envelope

The second test refers to the combined compression-shear stress state. Fig. 3 shows the failure envelope of the proposed model compared with the test results found by Goode and Helmy (1967). The analyses have been performed by initially imposing the axial strain ϵ_x and then increasing the shear deformation γ_{xy} while enforcing the transverse stresses σ_y to be zero. Application of the shear strain causes, in the nonlinear regime, an increase of the axial force due to the dilatancy of the material, followed by a simultaneous drop in both the shear and axial components when failure takes place (loss of internal cohesion, splitting).

Finally, in Fig. 4, the model's biaxial failure envelope is plotted and compared with the test results by Kupfer and Gerstle (1973). In the tension-tension and compression-tension quadrants, the model response is very accurate. In the biaxial compression zone, the model failure envelope deviates from the experimental one. This is, to a certain extent, a desirable feature for the intended use of the model, because in case of a large longitudinal compressive strain, the transverse steel tends to provide isotropic confinement independently of the orientation of the bending and shear forces, and therefore the model, although only bidimensional, must depart from the biaxial failure envelope of concrete to account for the out of plane confinement. For very high triaxial confinement, however, a full triaxial model with a deviatoric-volumetric splitting of the microplane response would be required to correctly describe the actual increase of resistance in the material, as, for example, in Bažant and Prat (1988).

STEEL

The stress-strain law used for the longitudinal steel fibers is based on the work of Menegotto and Pinto (1977). The model is well known and widely used as it provides an accurate prediction of the uniaxial tension-compression response of the reinforcing bars. The skeleton branch for the steel is divided in three parts: (1) A linear elastic branch; (2) a perfectly plastic one (i.e., yield plateau); and (3) a hardening branch.

The hardening branch is defined by the initial point and his tangent (ϵ_{sh}, σ_y, E_{sh}) and the ultimate strength point (ϵ_{su}, σ_{su}), where the tangent modulus is zero by definition

$$\sigma_s = \sigma_{su} + (\sigma_y - \sigma_{su}) \left| \frac{\epsilon_{su} - \epsilon_s}{\epsilon_{su} - \epsilon_{sh}} \right|^P; \quad P = E_{sh} \left(\frac{\epsilon_{su} - \epsilon_{sh}}{\sigma_{su} - \sigma_y} \right) \tag{6}$$

where σ_s and ϵ_s = current stress and strain values.

Unloading and reloading branches are defined instead by the following expression:

$$\sigma_s = \sigma_0 + (\epsilon_s - \epsilon_0) E_m \left[Q + \frac{1 - Q}{\left(1 + \left| E_m \frac{\epsilon_s - \epsilon_0}{\sigma_{ch} - \sigma_0} \right|^R \right)^{1/R}} \right] \tag{7}$$

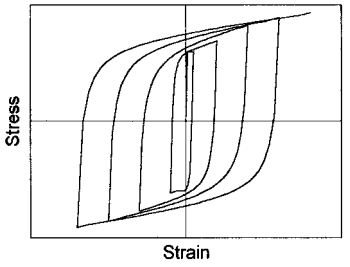

FIG. 5. Steel: Cyclic Behavior

where ϵ_0 and σ_0 = coordinates of the last reversal from the skeleton branch. The other parameters are used to define the shape of the curve and to impose the tangent passage to the new junction coordinates on the skeleton branches. E_m is the initial modulus of elasticity at reversal, σ_{ch} is a characteristic stress, Q is the ratio of the final tangent modulus to the initial one at reversal, and R is a curvature parameter; the larger R is the more the curve tends to be bilinear, when $R = 1$ the curve is hyperbolic.

At each reversal the origin of the skeleton branch is shifted based on the previous plastic deformation; this gives a set of different rules depending on whether the reversal takes place from the skeleton branch or from the unloading branch. A typical cyclic response of the model is plotted in Fig. 5.

Implementation of buckling and dowel effects in the steel subroutine is currently under way. These two mechanisms significantly affect the member behavior, particularly the latter mechanism, which does contribute to the shear resistance of the section, even at low damage levels.

SECTION MECHANICS

A better understanding of the resisting mechanisms of the model can be obtained by looking at the longitudinal, lateral, and shear strain field of a reinforced concrete (RC) section subjected to coupled axial, bending, and shear, as in Fig. 6.

Although based on the plain section hypothesis, the longitudinal stress field has proved to be accurate, even for squat elements. Rotation of the principal stress and strain directions does not alter significantly the longitudinal stress distribution, which, in fact, is almost insensitive to any variation in the shear strain field due to the use of one particular shape function instead of another. Most of the inaccuracy is caused instead by the localized slip of the reinforcement, which is only accounted for by the smeared tension softening branch of the concrete fibers.

Transverse strains and stresses depend on the amount of transverse steel, on the section geometry, and on the concrete dilatancy. The confining forces due to transverse steel can be evaluated with precision, their distribution within the section can also be accounted for, although in an empirical fashion, by specifying the ''effective'' confinement of each fiber. The concrete dilatancy is harder to depict, particularly that due to shear, which is mostly localized across the cracks and can be captured by the model in only a smeared sense.

Shear stresses are functions of shear strain and longitudinal and transverse confinement. Shear strains are predefined by the shear shape functions. Both parabolic and constant ones tend, in the nonlinear regime, to overestimate the shear deformations in the compression zone instead of shifting to the tensile zone to allow for a redistribution of the shear stresses in the conglomerate according to the equilibrium conditions (Vecchio and Collins 1998).

Shear transfer across the crack does not require a constitutive relation of its own as in discrete models; smeared models such as the microplane should automatically account for it. Because aggregate interlock is modeled as an inclined compression stress across the crack (compression stress with tensile strain), a transition branch between the tensile and compression branch of the microplane stress-strain laws is required, particularly at large strains (macrocracks). Calibration of this crack-bridging branch is beyond the objective of this paper and has therefore been omitted.

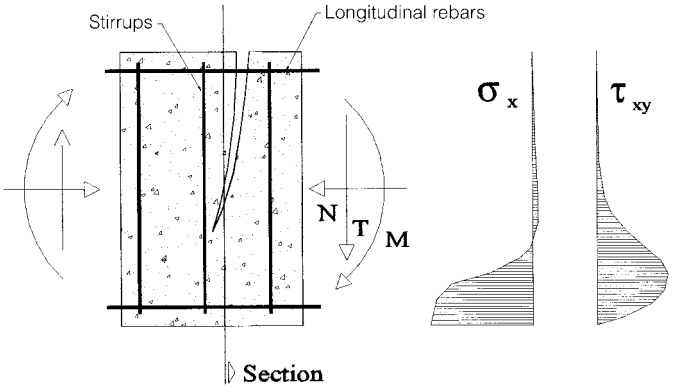

FIG. 6. Section Longitudinal and Shear Strain Field

As a result of the mechanisms discussed above, the proposed model yields a stress field where the shear stresses are mostly carried by the compression zone, what is in effect realistic (Fig. 6). The shear stress intensity is a function of the principal tensile resistance under predominant compression condition (material toughness) and of the longitudinal and transverse confinement. Because longitudinal stresses can be modeled with reasonable accuracy, the model shear response mainly depends on the concrete constitutive model and on the confining stress distribution, which is likely to be accurate in an average sense only (i.e., over the whole section). The result is somehow similar to a tensorial version of the strut and tie analogy, where interaction between axial, bending, and shear can be accounted for.

COLUMNS

Squat bridge piers have become a serious source of concern, particularly after the Hyogoken Nambu (Kobe) earthquake of 1995, as they are prone to shear-driven brittle failures. Similar failures are less likely to occur in RC frames of buildings made of slender members that can often rely on a number of other structural and nonstructural shear and vertical load-resisting elements. Squat piers are common in flyover structures where the height is the minimum required by the underneath clearance and the pier cross-section is conditioned by sometimes large permanent and traffic loads. The occurrence of short piers in bridges is also common when adapting to irregular soil profiles.

Most of the existing piers of this type, although shear sensitive, do normally have a shear resistance that is in excess of the bending resistance and therefore would fail in bending under monotonic loading. The abundant shear failures that have occurred during the 1995 Hyogoken Nambu earthquake were caused, in fact, by a much faster degradation of the shear resistance compared with the bending one. Typical of this situation is the case where the hoops are not properly anchored and cease working after concrete cover spalls at large ductility.

Given this scenario, the most realistic and interesting tests to analyze refer to columns that initially develop bending hinging, subsequently show significant shear deformations, and eventually fail. In these elements the interaction between axial, bending, and shear force is fundamental to the understanding of their behavior, as the bending not only provides the initial cracking, but also activates the confining effect of the hoops because of the lateral dilatancy of concrete.

The first example to be presented is a single pier tested in

the European Laboratory for Structural Assessment (ELSA) as part of a large-scale pseudodynamic campaign addressed to bridge structures designed to the new Eurocode 8 Part 2 EC8 for bridges in seismic areas (Pinto et al. 1996). The same example has been analyzed in detail by Pinto et al. (1995) and Ranzo and Petrangeli (1998), using different types of fiber beam elements.

The pier cross-sectional geometry and reinforcement details are shown in Fig. 7. The height was fixed at 2.8 m, and the axial load at N = 1,700 kN. Material properties for concrete were set, according to the experimental findings, as follows: Compressive strength = 35.4 MPa, tensile strength = 3.1 MPa, Young modulus = 29.4 MPa, and Poisson's ratio = 0.18, total fracture energy per unit length (meter) $\mathcal{G}_{tot}$ 2.0 kN. Steel properties (B500 Tempcore) are the following: Yield stress = 500 MPa, ultimate stress = 580 MPa, ultimate strain = 10%, and Young modulus = 200,000 MPa.

The total fracture energy per unit length has been fixed to roughly twice the energy found by dividing the concrete fracture energy ($\mathcal{G}_f$ = 0.1 kN/m) by an estimated crack spacing of 0.1 m as follows: $\mathcal{G}_{tot} = 2 \times 0.1/0.1$. This setting seems to provide a reasonable estimate of the total concrete fracture energy that is released at large strains. This energy must include, in addition to the fracture energy needed for crack opening, the bond energy released by diffuse microcracking of the concrete around the rebars. It is pointed out that these findings are not supported by specific tests aimed at evaluating the tension stiffening energy to be used in smeared models for RC structures, but only by the tests carried out by the writer on beams and columns with fiber elements with and without shear modeling.

The column under consideration, although having a shear span ratio of 1.75, with the longitudinal reinforcement ratio at 0.92% and transverse ratio at 0.68%, showed a ductile behavior. Significant diagonal cracking was observed, but the resisting mechanism has been flexure driven. Initial simulations (Fig. 8) that were carried out with the traditional fiber element (without shear modeling), were close enough, but the energy dissipation at load reversal was overestimated. This was first thought to be caused by the lack of proper modeling of the instabilities taking place in the longitudinal rebar, although, given the proper hoop arrangement, the explanation never seemed totally convincing. Subsequent simulations with the fiber model with shear modeling (Fig. 9) showed that when

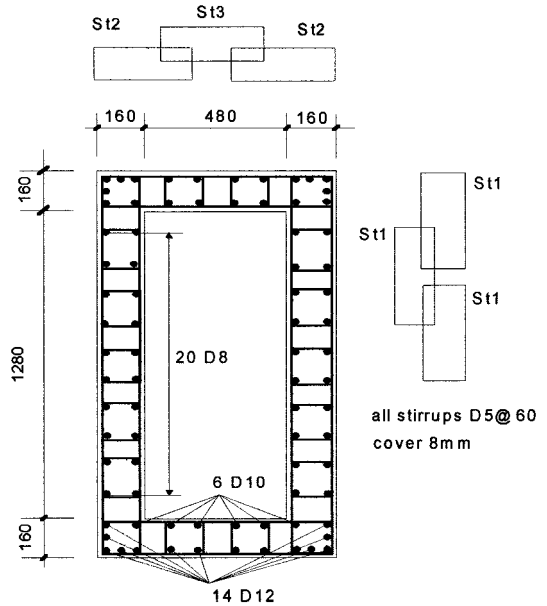

FIG. 7. ELSA Test: Cross-Sectional Geometry and Reinforcement Detail

the column developed bidiagonal cracks and the hoops yielded, shear deformability at load reversal was extremely large and it takes a large column shift before the shear resisting mechanism is activated.

In this displacement range, two mechanisms may introduce significant additional stiffness in a situation where, in case of zero axial force (no friction), the stiffness would be almost nonexistent. The first is the dowel effect, the second is caused by the relative displacement of concrete surfaces across large cracks (crack bridging), which tends to reduce the interval of zero stiffness of the shear mechanisms as highlighted in the experimental response in Fig. 9.

A further simulation makes use of the results on bridge piers tested at the University of Rome ''La Sapienza'' (De Sortis and Nuti 1996), as part of a pseudo-dynamic campaign aimed at comparing the new EC8 norm with the past Italian seismic code.

Two examples have been analyzed from a testing campaign involving a large number of pier specimens of different geometry and reinforcement layouts built at a 1:6 scale. These piers were meant to be representative of a four-span continuous bridge made of a prestressed concrete box girder. The two analyzed specimens refer to a squat pier with two different reinforcement layouts as shown in Fig. 10. Material properties for concrete were set as follows: Compressive strength = 22 MPa, tensile strength = 2.0 MPa, Young modulus = 28 MPa,

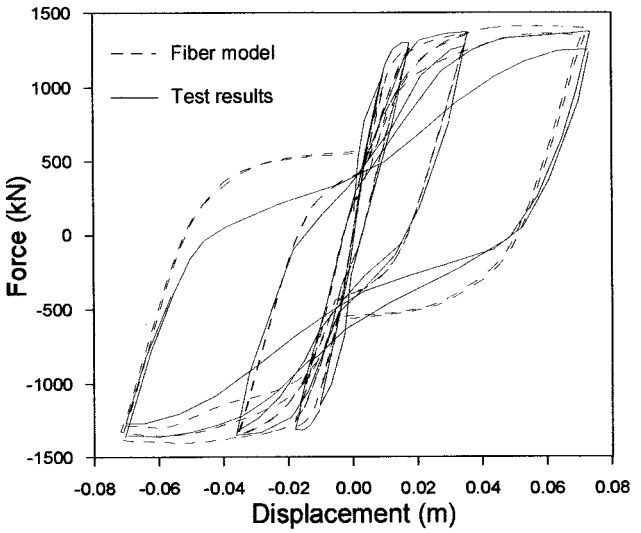

FIG. 8. ELSA Test: Flexural Fiber Model

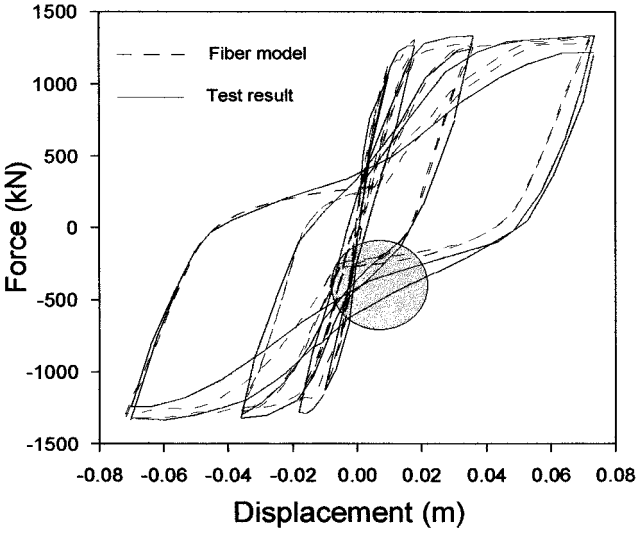

FIG. 9. ELSA Test: Fiber Model with Shear Modeling

Poisson's ratio = 0.18, and fracture energy per unit length (meter = 1.5 kN (Specimen B) and 2.0 kN (Specimen A). Steel properties were the following: Yield stress = 500 MPa, ultimate stress = 580 MPa, ultimate strain = 10%, and Young modulus = 200,000 MPa.

Both columns have performed satisfactory under an earthquake with a PGA of 0.35*g*, notwithstanding a substantial difference in their response. Specimen A, given the large amount of longitudinal reinforcement, experienced severe cracking of concrete along the whole height, resulting in an overall shear contribution to the total displacement in excess of 40%. Specimen B, because of the smaller amount of longitudinal reinforcement and associated shear and bending forces, remained uncracked except for the plastic hinge at the pier base. This difference, as far as the shear design is concerned, has an important significance. The results indicate that the shear forces carried by the concrete and the truss mechanism of hoops and ties do not overlap. Specimen A undergoes severe shear cracking before the resistance of the steel hoops, which is in excess of the bending forces (capacity design), is activated.

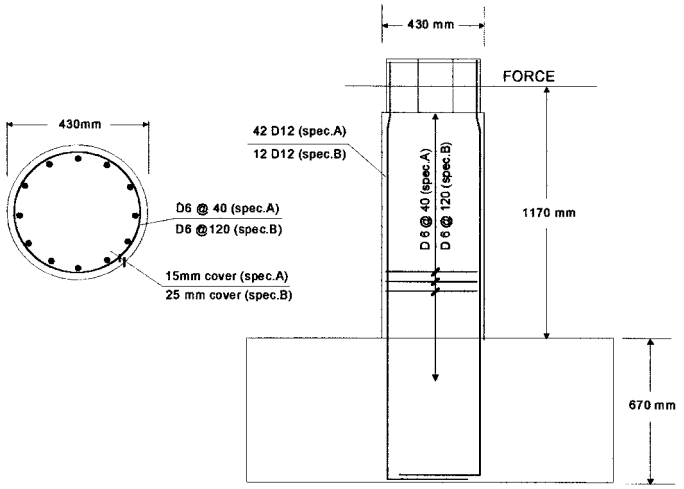

FIG. 10. Column Geometry and Reinforcement Details

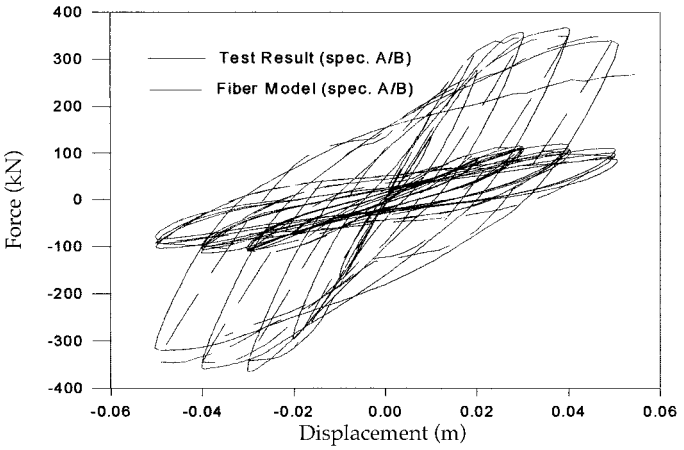

FIG. 11. Force-Displacement Response for Two Piers

The numerical results found with the model reproduce the experimental findings. The force-displacement responses are plotted in Fig. 11, comparing the experimental results with the numerical simulations for the two piers. Because these quasistatic tests were performed after the pseudodynamic simulations, the piers showed a degrated strength and stiffness that had to be accounted for in the numerical model, imposing two cycles at the same maximum amplitude (20 mm) reached by the two specimens during the previous tests. Yield penetration and bond slip should be included in the model as they account for a large percentage in the flexural degradation of the specimens.

The shear distortion at the integration points (sections) along the element are plotted in Fig. 12 at three different stages of the quasistatic test, showing the different shear response along their height. The shear distortion of Specimen B is almost zero outside the plastic hinge region because cracking does not cut through the section as in Specimen A. In this case, the shear distortion, following the initial cracking along the whole height, increases at the plastic hinge location only because of bending-shear degrading interaction while remaining constant elsewhere, because the maximum shear force does not increase during the analysis.

BEAMS

The capability of the model to predict the shear failure of RC beams under four-point bending is investigated. The results of the numerical analyses are compared with the experimental findings of the recent tests carried out by Kawano and Watanabe (1997) on similar beams of different sizes. A typical geometry of the specimen is plotted in Fig. 13. The beams have no web reinforcement and a longitudinal tensile reinforcement ratio of 1.3%. Material properties used in the model were fixed as follows: Compressive strength = 24 MPa, tensile strength = 2.2 MPa, Young's modulus = 30 MPa, Poisson's ratio = 0.18, fracture energy = 0.2 kN/m, and steel Young's modulus = 200,000 MPa. For these experiments, because the predominant cracking is limited to a single crack, each beam section has been given the same fracture energy per unit surface, which means that each section has been given a fracture

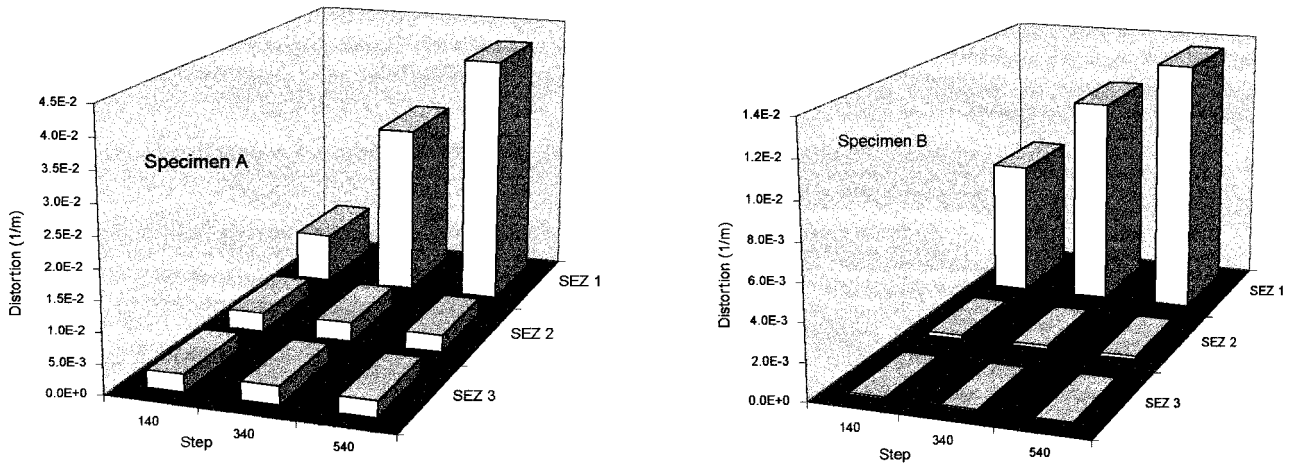

FIG. 12. Shear Distortion Along Height

energy per unit length equal to the above specified fracture energy divided by the section tributary length (i.e., the weight of the section using a Gauss integration scheme). This approach is the 1D equivalent to the so-called ''crack band approach'' used in the 2D analysis of concrete structures (Bažant and Oh 1983); although in this case the band length is generally shorter than the beam length as the damage, using the equilibrium-based approach discussed in the companion paper, localizes in a single section.

All of the specimens were modeled using three elements, each with four integration points. An initial lack of symmetry was introduced to trigger the correct antisymmetric shear failure mechanism observed in the experiments. Consequently, all of the specimens developed flexural cracks at the various sections along the model and then experienced brittle shear failure at one of the two sections adjacent to the point loads. These results confirm the experimental finding that the final cracks extended toward the load application points, where shear failure of the compression zone caused the collapse of the beams.

Beam resistance at different sizes, taking into account the specimen self-weight, are plotted in Fig. 14. The results are represented on a logarithmic scale in terms of nominal shear stress $\tau = P/bd$ versus beam depth d.

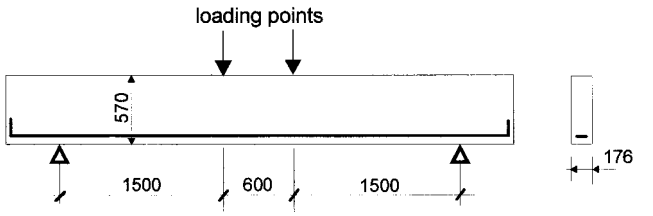

FIG. 13. Geometry and Loading

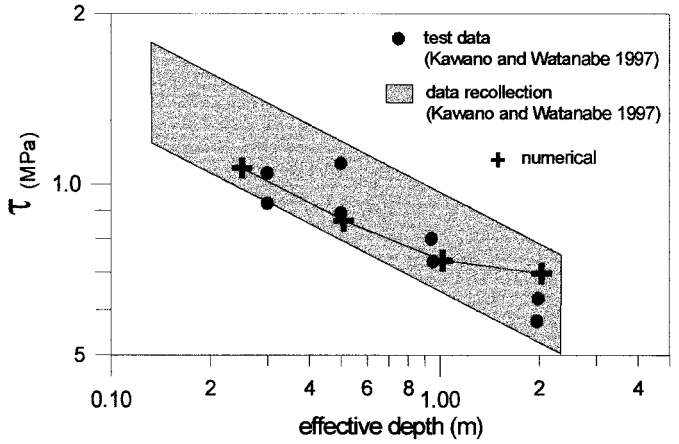

FIG. 14. Size Effect on Beam Shear Strength

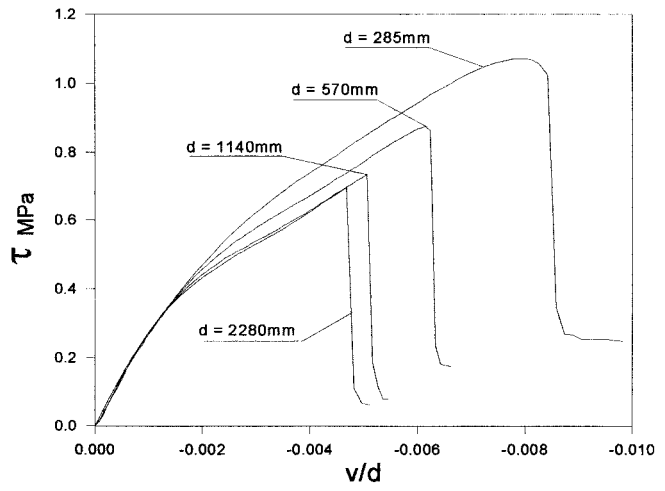

FIG. 15. Normalized Force Displacement Response

It can be seen that the model predicts a significant size effect for small-size specimens and an asympstotic strength of the beam shear resistance at large sizes. Due to the brittleness of the failure mechanism and the assigned section kinematic, large beam failures tend to take place at the same stress level, independent of the size. The possibility of departure from the size effect law (Bažant 1984) for large specimen sizes has been suggested by other researchers as well (Ožbolt and Eligehausen 1996), as it finds some evidence in both 2D finite-element simulations and laboratory tests.

For the proposed model, the tendency of the failure load to approach a strength criterion is not surprising, a different result would be impossible, as long as the same material properties, a constant fracture energy, and no initial flaw in the specimens, are specified. In the smaller specimen the fracture energy is enough to postpone the section collapse by stress redistribution and therefore yield higher nominal shear stresses. The response in terms of nominal shear stress versus normalized displacement (displacement over effective depth) is plotted in Fig. 15.

The satisfactory prediction of the shear resistance for small-sized beams proves the capability of the model to predict the behavior of RC beams, even with a low span ratio, except when unstable crack propagation takes place as, for example, in large specimens without reinforcement. In this case, the uniaxial model obviously becomes inappropriate and a 2D model should be used instead.

STRUCTURAL ASSESSMENT AND DIAGNOSIS

A simple application of the proposed model to the viaduct's failure of the 18-span segment along the Kobe Route 3 of the Hanshin expressway during the last Hyogoken Nambu earthquake is proposed. The collapse of this viaduct is very interesting as it appears that the causes of it are to be found in a compression-driven shear failure due to coupling of axial, bending, and shear forces. Preliminary investigations carried out using the purely flexural fiber beam element could not explain the toppling of the viaduct because the displacements were too small to trigger significant P-Delta effects.

The pier geometry and cross section are plotted in Fig. 16. It can be seen that the piers had the inner longitudinal rebar layer together with the inner hoop one interrupted at roughly 2.5 m above the foundation. This interruption weakened the piers to the extent that the failure took place at this section instead of the base one. Close scrutiny of the structure after the earthquake showed, among other things, that the hoops of the collapsed section had opened up because of poor anchorage detailing. The hoops' anchorage was obtained by simply

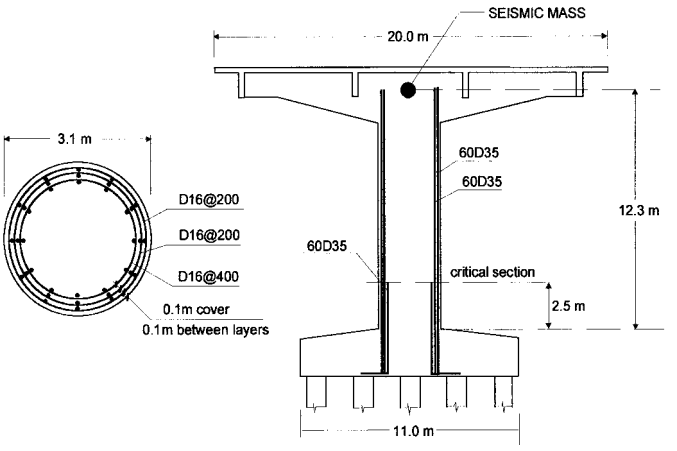

FIG. 16. Hanshin Column Piers

overlapping the rebars without bending them inside the section core. Therefore, spalling of the outer concrete must have caused loosening of the hoops and longitudinal rebar buckling.

These and other phenomena were clarified by performing a number of analyses with the proposed model. A four-element finite-element mesh has been set up with a translational and rotational mass lumped at the pier top to simulate a one-span deck translational inertia at 1,100 kN and a rotational one at 29,000 kNm^2. Different configurations have been analyzed investigating the effect of the longitudinal and transverse steel interruption as well as the effect of hoop anchorage on the pier performance.

The structure has been subjected to the north-south component of the Kaiyou Weather Bureau accelerograms with a

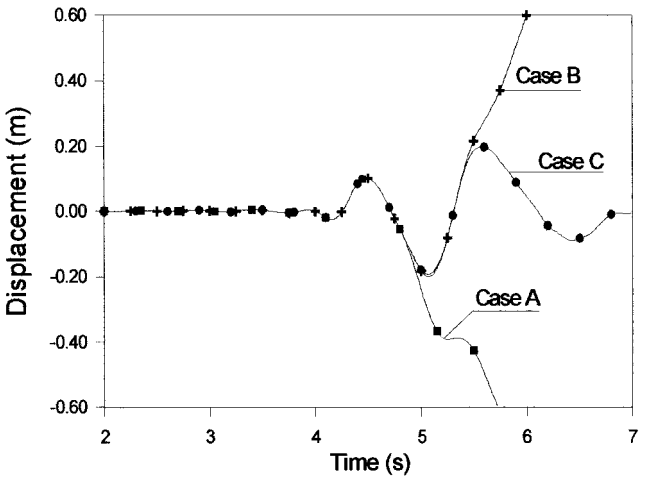

FIG. 17. Pier Top Displacement History

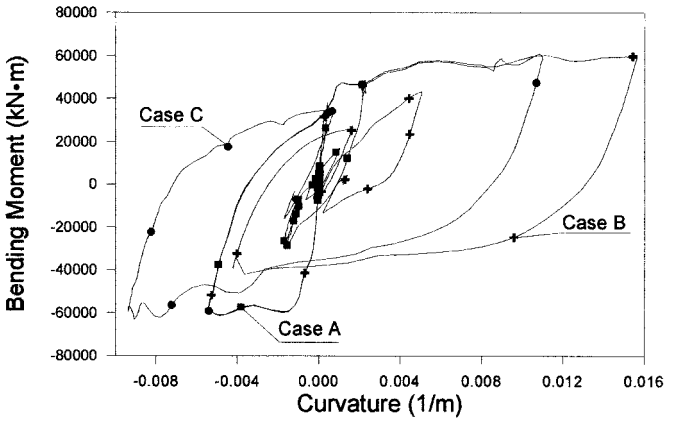

FIG. 18. Moment—Curvature of Weak Section

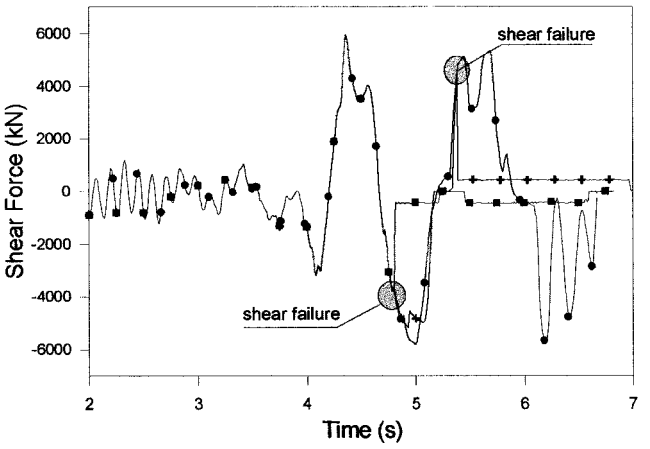

FIG. 19. Section Shear Force History

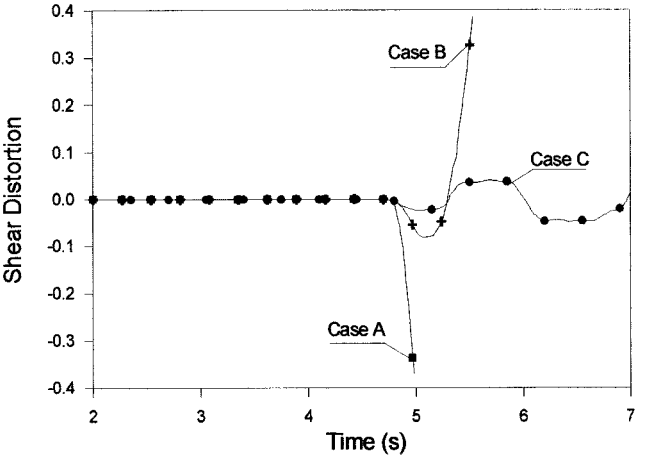

FIG. 20. Section Shear Distortion History

PGA equal to 0.81*g*. Mechanical properties of the concrete are: Compressive strength = 30 MPa, Young's modulus = 30,000 MPa, tensile strength = 25 MPa, and fracture energy per unit length varied from 1.5 to 0.8 kN. Mechanical properties of the steel are the following: Yield strength = 350 MPa, ultimate strength = 450 MPa (380 MPa for the hoops), Young's modulus = 200,000 MPa, and ultimate strain = 0.12. The transverse steel area attributed to the concrete core fibers is equal to the corresponding hoop area per unit length (50 cm^2/m up to the inner hoop layer interruption and 40 m^2/m above).

Fig. 17 shows the pier top displacement of three different configurations, namely, the existing situation with a hoop strain cut off to simulate the loss of anchorage at 1% elongation (Case A), the same situation without hoop cut of strain (Case B), and one without transverse hoop interruption and without hoop cutoff strain (Case C). The results of the actual configuration (Case A) with poor hoop anchorage shows that the structure must have collapsed immediately after the first cycle at large ductility, as also shown by the moment curvature of the collapsed section plotted in Fig. 18. The results of Cases B and C show instead that with proper hoop anchorage the piers would have remained intact or nearly so, or at least as a small increment of transverse steel (Case C) seems enough to prevent the toppling of the viaduct.

Shear force and shear distortion time histories for the weak section (Figs. 19 and 20) show clearly the shear failures that take place in Cases A and B.

CONCLUSIONS

The capability of the proposed model to predict the behavior of RC beams and columns for a wide range of configurations and loading histories seems to represent a significant step forward with respect to other existing finite-beam elements. This has been obtained by compiling various results achieved in different fields of computational mechanics by the writer as well as other researchers. The main contributions can be summarized as follows:

- A new solution strategy for the nonlinear beam has allowed for the efficient integration of spread material nonlinearities in both a hardening and softening regime with accuracy and extreme robustness. This algorithm has also allowed for a reduction of the monitoring stations (sections) to be located along the element and have increased the allowable loading step during the analysis.
- A biaxial concrete constitutive model based on a modified microplane approach has provided an efficient numerical tool for the simulation of concrete behavior under a sufficiently wide range of stress-strain paths in both mono-

tonic and cycling loading. No other approach, to the writers knowledge, could have provided the same performance/computational cost ratio in the cyclic range.
- The fiber beam approach, in the proposed new extension to the shear modeling, provides a satisfactory compromise between modeling accuracy and user friendliness. Different geometry and reinforcement configurations can be easily set up, reducing input and computing time dramatically.

Within the limit of the monodimensional schematization, the proposed beam element provides a further insight into the damage mechanisms that take place in RC beams and columns when subjected to large alternate deformations, although the full potential of the model is better appreciated with analyses on larger structures where the interest is more focused on the structural response than on the details of the members' failure mechanisms. Analyses of this kind have not been presented in this paper as they do not contribute to the understanding of the model behavior, although they are being carried out in various applications showing the potential of the algorithm.

ACKNOWLEDGMENTS

Partial financial support for the underlying studies was received from the Structural and Geotechnical Department of the University of Rome ''La Sapienza'' and the Institut für Werkstoffe im Bauwesen, Universität Stuttgart. Valuable discussions and interesting examples have been collected by the writer during an invitation by the Public Work Research Institute in the Kobe area and at the PWRI headquarters in Tsukuba, Japan.

APPENDIX. REFERENCES

Bažant, Z. P. (1984). ''Size effect in blunt fracture: Concrete, rock, metal.'' *Mat. and Struct.*, Paris, 16(93), 155–177.

Bažant, Z. P., and Oh, B. H. (1983). ''Crack band theory for fracture of concrete.'' *J. Engrg. Mech.*, ASCE, 110(4), 518–535.

De Sortis, A., and Nuti, C. (1996). ''Seismic response by pseudo-dynamic tests of RC bridges designed to EC8.'' *Proc., 11th World Conf. on Earthquake Engrg.*

Goode, C. D., and Helmy, M. A. (1967). ''The strength of concrete under combined shear and direct stress.'' *Mag. of Concrete Res.*, 19(59), 105–112.

Kawano, H., and Watanabe, H. (1997). ''Shear strength of reinforced concrete columns—Effect of specimen size and load reversal.'' *Proc., 2nd Italy-Japan Workshop on Seismic Des. and Retrofit of Bridges.*

Kupfer, H. B., and Gerstle, K. H. (1973). ''Behaviour of concrete under biaxial stresses.'' *J. Engrg. Mech. Div.*, ASCE, 99(4), 853–866.

Mander, J. B., Priestley, J. N., and Park, R. (1988). ''Theoretical stress-strain model for confined concrete.'' *J. Struct. Engrg.*, ASCE, 114(8), 1804–1826.

Martinez-Rueda, J. E., and Elnashai, A. S. (1997). ''Confined concrete model under cyclic load.'' *Mat. and Struct.*, Paris, 30, 139–147.

Menegotto, M., and Pinto, P. E. (1977). ''Slender RC compressed members in biaxial bending.'' *J. Struct. Div.*, ASCE, 103(3), 587–605.

Ožbolt, J., and Eligehausen, R. (1996). ''Size effect in concrete and RC structure—Diagonal shear and torsion.'' *Studi e ricerche*, Italcementi S.p.A., eds., 17, 37–67.

Petrangeli, M. (1996). ''Modelli numerici per strutture monodimensionali in cemento armato,'' PhD dissertation, University of Rome ''La Sapienza,'' Rome (in Italian).

Petrangeli, M., Pinto, P. E., and Ciampi, V. (1999). ''Fibre element for cyclic bending and shear of RC structures. I: Theory.'' *J. Engrg. Mech.*, ASCE, 125(9), 994–1001.

Pinto, A. V., Verzelletti, G., Negro, P., and Guedes, J. (1995). ''Cyclic testing of a squat bridge-pier.'' *Rep. EUR 16247 EN, EC, JRC*, Ispra, Italy.

Pinto, A. V., Verzelletti, G., Pegon, P., Magonette, G., Negro, P., and Guedes, J. (1996). ''Pseudo-dynamic testing of large-scale R/C bridges.'' *Rep. EUR 16378 EN, EC, JRC*, Ispra, Italy.

Popovics, S. (1973). ''A numerical approach to the complete stress-strain curves of concrete.'' *Cement and Concrete Res.*, 3(5), 583–599.

Ranzo, G., and Petrangeli, M. (1998). ''A fibre beam element with section shear modelling for seismic analysis of RC structures.'' *J. Earthquake Engrg.*, 2(3), 443–473.

Sinha, B. P., Gerstle, K. H., and Tulin, L. G. (1964). ''Stress-strain relations for concrete under cyclic loading.'' *J. Am. Concrete Inst.*, 62(2), 195–210.

van Mier, J. G. M. (1986). ''Multiaxial strain-softening of concrete. Part I: Fracture. Part II: Load histories.'' *Mat. and Struct.*, 111(19), 179–200.

Vecchio, F. J., and Collins, M. P. (1988). ''Predicting the response of reinforced concrete beams subjected to shear using modified compression field theory.'' *ACI Struct. J.*, May–June, 258–268.